Degradation mechanism of perovskite $CH_3NH_3PbI_3$ diode devices studied by electroluminescence and photoluminescence imaging spectroscopy

Applied Physics Express 8, 102302 (2015)
http://dx.doi.org/10.7567/APEX.8.102302

Degradation mechanism of perovskite $CH_3NH_3PbI_3$ diode devices studied by electroluminescence and photoluminescence imaging spectroscopy

Makoto Okano[1†], Masaru Endo[1], Atsushi Wakamiya[1], Masahiro Yoshita[2,3], Hidefumi Akiyama[2,3], and Yoshihiko Kanemitsu[1,3*]

[1]*Institute for Chemical Research, Kyoto University, Uji, Kyoto 611-0011, Japan*
[2]*Institute for Solid State Physics, University of Tokyo, Kashiwa, Chiba 277-8581, Japan*
[3]*Japan Science and Technology Agency, CREST, Uji, Kyoto 611-0011, Japan*
E-mail: kanemitu@scl.kyoto-u.ac.jp

Received August 25, 2015; accepted September 14, 2015; published online October 2, 2015

We investigate the degradation behavior of non-sealed perovskite $CH_3NH_3PbI_3$ diode devices in air at room temperature by means of electroluminescence (EL) and photoluminescence (PL) imaging techniques. From the comparison of these images, we determine that the spatial fluctuation of the EL intensity is mainly due to fluctuations in the luminescence efficiency of the perovskite layer itself. By applying a constant voltage for tens of minutes, the EL intensity decreases gradually. It is observed that the temporal evolution of the EL intensity is governed by the degradation of the perovskite layer and the carrier injection at the interface. © 2015 The Japan Society of Applied Physics

Organic–inorganic hybrid thin-film solar cells consisting of perovskite materials, such as $CH_3NH_3PbI_3$, have been considered as possible candidates for the development of emerging thin-film solar-cell technology because of their high conversion efficiencies of over 20%.[1)] This is comparable with the efficiency of multinary-semiconductor-based solar cells, which show the highest conversion efficiency among thin-film solar cells.[2)] In addition, perovskite materials have other advantages, such as simple and easy fabrication by solution processes.[3)] Therefore, during the last few years, numerous studies have been conducted on improving the efficiency and stability of such solar cells as well as understanding the electrical and optical properties of perovskite semiconductors.[1,3–12)] The efforts on the former issue seem to have succeeded, as evidenced by the fact that solar cell efficiency has promptly increased from 3.8 to 20%.[1,3)] Moreover, because of the notable optical properties of perovskite $CH_3NH_3PbI_3$ materials, their applications in other optoelectronic devices, such as light-emitting devices (LEDs) show promise.[9–12)] However, the rapid degradation of perovskite diode devices is a serious issue for practical applications.[13–17)] Thus, a clear understanding of the fundamental properties and the degradation mechanism of perovskite diode structures will allow us to optimize the structures of perovskite-based solar cells and LEDs.

Recently, various optical techniques have been adopted to reveal the photoelectric conversion processes of solar-cell materials and devices.[18–21)] In particular, a combination of different optical methods is useful in understanding the optical and electronic properties of complicated perovskite materials and solar cells.[18–23)] Concerning device structure, electroluminescence (EL) measurements are one of the most powerful techniques for gaining deeper insights into the photoelectric conversion processes because the EL process is perfectly related with the photovoltaic process through a reciprocal relationship.[24)] Indeed, EL measurements have been widely used in the context of Si-, GaAs-, $Cu(In,Ga)Se_2$-, and perovskite-based solar cells on account of the impressive correlation between EL properties and photoconversion efficiency.[11,25–28)] Moreover, EL and photoluminescence (PL) images enable us to investigate the spatial homogeneity of perovskite solar cells and LEDs that are composed of crystal grains and boundaries. Studies on EL intensity degradation also provide useful indications for the understanding of the degradation mechanisms of solar cells. Therefore, a combination of space- and time-resolved EL and PL imaging spectroscopy is essential for unveiling the degradation process of perovskite diode devices such as solar cells and LEDs.

In this Letter, we report the bias-voltage dependence and the time evolution of EL images in perovskite $CH_3NH_3PbI_3$ solar cells and discuss their degradation mechanisms under EL operation. The spatial inhomogeneity of the EL intensity is mainly caused by the luminescence efficiency of the perovskite thin film itself. A monotonic decrease in the EL intensity is observed during application of the bias voltage, which causes a reduction in the luminescence intensity, even in the absence of sunlight illumination. Moreover, by comparing the EL and PL images, we distinguish the degradation caused by radiative recombination from the change of the charge-transport processes in devices under bias voltage. We conclude that the gradual and significant degradation of the EL intensity is mainly determined by the decrease in the radiative efficiency of the perovskite layer; on the other hand, the rapid variation of the EL intensity is caused by the temporal changes in the electrical properties of the interface between the perovskite and the charge-transport layers.

Figure 1(a) contains a schematic diagram of the perovskite $CH_3NH_3PbI_3$ sample used in this study. The non-sealed samples consisted of a fluorine-doped tin oxide (FTO) electrode, a ~30 nm compact TiO_2 layer, a ~320 nm mesoporous TiO_2 layer, a ~300 nm perovskite $CH_3NH_3PbI_3$ layer, a ~230 nm hole-transport-material (HTM) layer, and a thin Au electrode. The perovskite diode samples were fabricated by the two-step method.[20,29)] Because the strong impact of the HTM layer on solar cell performance has been pointed out in previous studies,[30–32)] we prepared two samples having different HTM layer thicknesses, ~230 and ~460 nm. The current–voltage (I–V) characteristics of the perovskite solar cells under 1-sun illumination are plotted in Fig. 1(b). Because it has been demonstrated that the I–V characteristics of perovskite solar cells are affected by the scan rate and direction,[33)] we fixed the scan rate at 0.05 V/s; the applied bias voltage was first increased from −0.1 to 1.1 V and then

[†]Present address: Department of Physics, Keio University, Yokohama 223-8522, Japan.

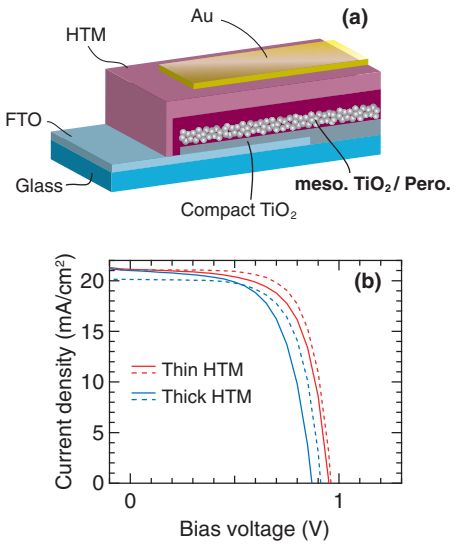

Fig. 1. (a) Schematic diagram of the perovskite $CH_3NH_3PbI_3$ solar cells. (b) Photocurrent density vs bias voltage of perovskite samples with thin (red curves) and thick (blue curves) HTM layers under 1-sun illumination at a scan rate of 0.05 V/s. Forward and backward scans of bias voltage are represented by solid and dotted curves, respectively.

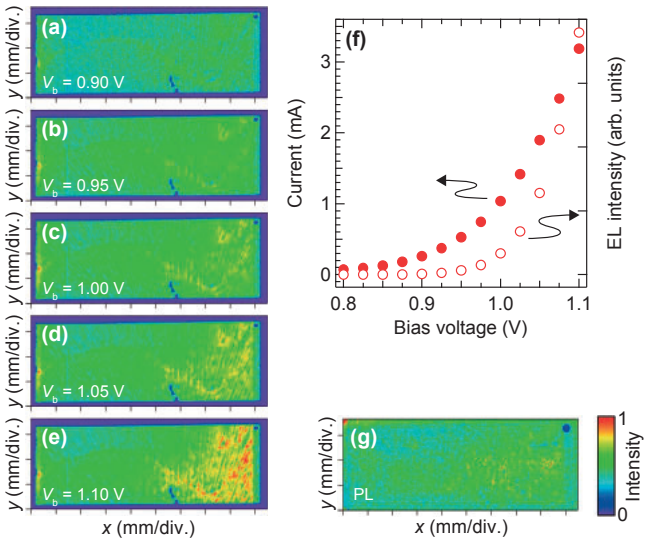

Fig. 2. (a)–(e) Bias-voltage dependence of the EL images of the thin-HTM-layer $CH_3NH_3PbI_3$ samples. (f) Current (filled circles) and EL intensity (open circles) plotted as a function of bias voltage. (g) PL image of the $CH_3NH_3PbI_3$ sample.

decreased from 1.1 V to −0.1 V. It was observed that the *I*–*V* characteristics of the two samples showed weak hysteresis behavior. The solar cell efficiencies of the thin- and thick-HTM-layer samples were estimated to be approximately 13.8 and 12.0%, respectively.

To investigate the spatial inhomogeneity of the perovskite devices, we performed EL and PL imaging measurements. In these measurements, the EL and PL emissions through the glass substrates were detected by a CMOS sensor with a camera lens. For the PL measurements, a laser diode with a wavelength of 635 nm (∼1.95 eV) was used as an excitation source. The EL and PL spectra of our samples had a single-peak structure with a peak wavelength of ∼770 nm and a width of ∼50 nm; therefore, we selectively collected the EL and PL emission using long- and short-pass filters with cut-off wavelengths of 750 and 800 nm, respectively. Before applying the forward bias voltage, we set the bias voltage to −1.5 V until the current stabilized. In the PL measurements, the excitation-laser spot was elliptical and its size was estimated to be approximately $5 \times 20\,mm^2$ by the scattering of the excitation laser. The spot size was larger than the electrode, which had dimensions of $3 \times 9\,mm^2$. In order to rapidly monitor the degradation of the perovskite samples, all measurements were carried out in air at room temperature.

Figures 2(a)–2(e) show the bias-voltage dependence of the EL images in the thin-HTM perovskite sample. The EL intensities in all images are normalized to the highest EL intensity of each image. All EL emissions were observed only from a rectangular region, corresponding to the perovskite layer sandwiched between the FTO and the rectangular Au electrodes. This clearly indicates that the current only flowed in the normal direction to each constituent layer. At $V_b = 0.9$ V, the right part of the region of interest showed stronger EL than the left part [see Fig. 2(a)]. In addition, we observed no emission from the top-right corner and around the bottom-center edge; these dark spots were caused by defects in the perovskite layer. As the bias voltage increased, these features of the EL emission were maintained, as shown in Figs. 2(b)–2(e). The bias-voltage dependence of the current and EL intensity are plotted in Fig. 2(f). The EL intensity was derived from the spatial integration of the EL emission over the area investigated in the EL images. Above $V_b = 1.0$ V, the EL intensity increased more rapidly than the current. This can explain the increasing degree of inhomogeneity in the EL intensity as the bias voltage increases, as shown in Figs. 2(a)–2(e).

We also performed PL measurements of the perovskite diodes to separately investigate the spatial uniformity of the electric properties (i.e., charge injection and transport) as well as the optical properties. The EL intensity is governed by both the charge transport of the entire device and the radiative recombination of the perovskite layer. On the other hand, the PL intensity is governed only by the latter, because the perovskite layer can be selectively excited under an excitation of 1.95 eV in our device structures. The PL image of the sample shown in Figs. 2(a)–2(e) is displayed in Fig. 2(g). The observation of the PL emission was not limited to the rectangular region — i.e., the electrode — because laser irradiation can excite the perovskite material outside the electrode area and thus generate radiative recombination in these regions. Interestingly, we observed that the spatial distribution of the PL intensity is strongly correlated to that of the EL intensity; for example, the strong and weak intensity regions are located in the right and upper left regions, respectively, in both the EL and PL images. This obviously indicates that the spatial distribution of the EL intensity is mainly due to the spatial inhomogeneity of the luminescence efficiency in the perovskite layer itself.

To reveal the degradation mechanism of perovskite devices, we measured the temporal change of the EL intensity while applying a constant bias voltage of $V_b = 1.0$ V. Figures 3(a)–3(h) show the EL images for various elapsed times ranging from 0 to 30 min. In this experiment, we acquired the EL images with an exposure time of 5 s every 1 min. These EL images are normalized to the intensity

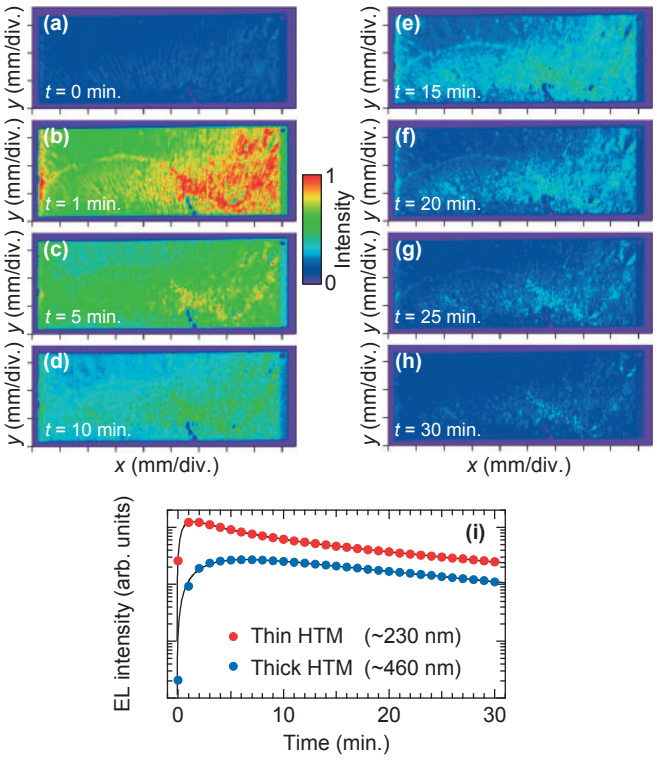

Fig. 3. (a)–(h) EL images of the thin-HTM-layer $CH_3NH_3PbI_3$ sample at different elapsed times after applying $V_b = 1.0$ V. (i) EL intensity of $CH_3NH_3PbI_3$ devices with different HTM thicknesses against elapsed time. The solid curves are guides for the eye.

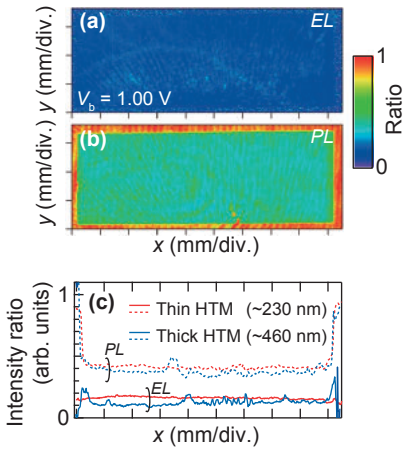

Fig. 4. Spatial distributions of (a) ratio of EL intensities before and after degradation and (b) ratio of PL intensities before and after degradation in the thin-HTM-layer perovskite devices. (c) Line profiles of EL (solid curves) and PL (broken curves) intensity ratios parallel to the *x*-axis of (a) and (b). The red and blue curves correspond to the perovskite devices with thin and thick HTM layers, respectively. These intensity ratios are averaged along the *y*-axis of the images.

shown in Fig. 3(b). As displayed in Fig. 3(a), the EL intensity was remarkably weak immediately after applying the bias voltage. The strongest EL intensity was observed after 1 min, after which it decreased in a monotonic fashion [Figs. 3(b)–3(h)]. Similar behaviors have also been observed in perovskite LEDs.[17] This decrease of the EL intensity can be attributed to the degradation of the perovskite devices. Note that the reduction of the EL intensity after 30 min was not recovered by introducing a time interval with zero bias voltage or by applying the reverse bias voltage in air at room temperature (data not shown); this indicates the occurrence of irreversible degradation in the perovskite layer.

Here, we focus on the spatial patterns acquired at different elapsed times to understand the degradation process in perovskite devices. As shown in Fig. 3(b), at 1 min, stronger EL emission was observed on the right side of the emission region. As the elapsed time increased, the EL emission from the right side remained stronger than that from the left side. If a higher current could induce stronger degradation, the right side would exhibit a faster decrease of the EL emission than the left side. Therefore, the degradation of the EL efficiency is not determined by the current density, which is linked to sample heating.

To evaluate the impact of the thickness of the HTM layer on the degradation of perovskite devices, we compared the EL intensities of the samples with the 230- and 460-nm-thick HTM layers at different elapsed times; the results are summarized in Fig. 3(i). In both samples, an initial rise in the temporal profiles of the EL intensity can be clearly observed. Subsequently, the EL intensities decrease monotonically until 30 min have elapsed. From 15 to 30 min, both perovskite devices show a similar reduction in the EL intensity. The rise time of the thick-HTM-layer sample (~3.6 min) was measured to be longer than that of the thin-HTM-layer sample (~0.52 min). In the thin-HTM-layer sample, we also observed a fast decay component with a lifetime of several minutes, which is comparable with the rise time of the thick-HTM-layer sample. These findings indicate that the HTM thickness is an important factor in the rise and decay of the EL intensity at the initial stage in perovskite devices.

We believe that the rise in the EL intensity is related to the accumulation of charges at the interface between the perovskite and the HTM layer. Because the mobility of the HTM layer is much smaller than that of the perovskite layer,[34] the charge accumulation in the HTM layer might modulate the charge injection at the interface. Thus, we consider that the rise time of the EL intensity is determined by the temporal change of the carrier injection into the HTM layer and the rapid degradation of the sample in air. On the other hand, the decrease of the EL after 15 min appears to be governed by the degradation of the perovskite layer itself, i.e., the increase of the nonradiative recombination in the perovskite; this is because the nonradiative Shockley–Read–Hall and Auger recombination processes increase with the carrier density in the sample owing to charge accumulation.[35–37]

To examine the degradation mechanism in more detail, we compared the emission intensity profile of the EL and PL images before and after degradation (i.e., after the EL measurements, while applying a bias voltage of 1.0 V for 30 min). Figures 4(a) and 4(b) show the maps of the EL and PL intensity ratios before and after degradation of the thin-HTM-layer sample. The degradation of the EL intensity at 1.0 V seems to occur uniformly, in contrast to the spatial distribution of the EL intensity. On the other hand, the degradation of the PL intensity shows large differences between the areas under the electrode and outside the electrode. Specifically, the PL intensity ratio under the electrode was ~0.4, whereas outside the electrode it was approximately unity, indicating that no significant degradation of the radiative efficiency of the perovskite layer occurred in air without current flow. These observations provide clear evidence that electrical

operation causes degradation of the perovskite materials. It should be emphasized that the EL intensity ratio was smaller than the PL intensity ratio everywhere.

Here, we discuss the degradation tendency of the PL and EL intensities of the two samples with different HTM layer thicknesses under bias voltage. The averaged intensity ratios along the *y*-axis are plotted as a function of *x* in Fig. 4(c). In these samples, the PL and EL intensity ratios were almost equal at every *x*-position and decreased to ∼0.4 and ∼0.2, respectively. This discrepancy means that the degradation of the EL intensity cannot be explained only by the increase of nonradiative carrier recombination in the perovskite layer. Thus, we believe that the difference between the EL and PL intensity ratios corresponds to the influence of the electric processes (i.e., charge injection and transport under an applied bias voltage) on the degradation. The deterioration of electric efficiency accounts for approximately one-fourth of the total degradation of perovskite diode structures, indicating the strong impact of electric properties on the EL process. This is plausible in perovskite diode structures with low external quantum efficiency.[17] Moreover, no notable discrepancy was observed between the two samples in terms of EL and PL intensity ratios. It is surprising that the degradation of the perovskite samples at or above 30 min is independent of the thickness of the HTM layer, despite the different temporal profiles of EL intensity displayed in Fig. 3(i). This implies that the temporal response at the early stages is strongly correlated with the HTM thickness, whereas the degradation at later times is determined by the heterointerfaces, which play an important role in charge-carrier transport. In order to suppress the degradation of device performance during operation in air, it is necessary to improve the quality of the perovskite layer and to control the heterointerfaces between the perovskite and the other layers.

In conclusion, we studied the degradation mechanism of non-sealed perovskite $CH_3NH_3PbI_3$ diode devices by using a combination of EL and PL imaging measurements. The spatial distributions of the EL and PL intensities were almost identical and were determined by the spatial fluctuation of the perovskite luminescence efficiency. Moreover, we observed that the bias-voltage operation in air at room temperature induces the degradation of the luminescence and electronic properties. The comparison between two samples with thin and thick HTM layers demonstrated that the degradation of the perovskite layer itself under bias voltage mainly determines the EL intensity degradation of perovskite solar cells.

Acknowledgments The authors thank Y. Yamada and T. Handa for discussions. This work was supported by The Sumitomo Electric Industries Group CSR Foundation (to M.O. and Y.K.), and JST-CREST (to Y.K.).

1) W. S. Yang, J. H. Noh, N. J. Jeon, Y. C. Kim, S. Ryu, J. Seo, and S. I. Seok, Science **348**, 1234 (2015).
2) P. Jackson, D. Hariskos, R. Wuerz, O. Kiowski, A. Bauer, T. M. Friedlmeier, and M. Powalla, Phys. Status Solidi: Rapid Res. Lett. **9**, 28 (2015).
3) A. Kojima, K. Teshima, Y. Shirai, and T. Miyasaka, J. Am. Chem. Soc. **131**, 6050 (2009).
4) H.-S. Kim, C.-R. Lee, J.-H. Im, K.-B. Lee, T. Moehl, A. Marchioro, S.-J. Moon, R. Humphry-Baker, J.-H. Yum, J. E. Moser, M. Grätzel, and N.-G. Park, Sci. Rep. **2**, 591 (2012).
5) M. M. Lee, J. Teuscher, T. Miyasaka, T. N. Murakami, and H. J. Snaith, Science **338**, 643 (2012).
6) N.-G. Park, J. Phys. Chem. Lett. **4**, 2423 (2013).
7) J. Burschka, N. Pellet, S.-J. Moon, R. Humphry-Baker, P. Gao, M. K. Nazeeruddin, and M. Grätzel, Nature **499**, 316 (2013).
8) Q. Chen, H. Zhou, Z. Hong, S. Luo, H.-S. Duan, H. H. Wang, Y. Liu, G. Li, and Y. Yang, J. Am. Chem. Soc. **136**, 622 (2014).
9) G. Xing, N. Mathews, S. S. Lim, N. Yantara, X. Liu, D. Sabba, M. Grätzel, S. Mhaisalkar, and T. C. Sum, Nat. Mater. **13**, 476 (2014).
10) F. Deschler, M. Price, S. Pathak, L. E. Klintberg, D.-D. Jarausch, R. Higler, S. Hüttner, T. Leijtens, S. D. Stranks, H. J. Snaith, M. Atatüre, R. T. Phillips, and R. H. Friend, J. Phys. Chem. Lett. **5**, 1421 (2014).
11) K. Tvingstedt, O. Malinkiewicz, A. Baumann, C. Deibel, H. J. Snaith, V. Dyakonov, and H. J. Bolink, Sci. Rep. **4**, 6071 (2014).
12) Z.-K. Tan, R. S. Moghaddam, M. L. Lai, P. Docampo, R. Higler, F. Deschler, M. Price, A. Sadhanala, L. M. Pazos, D. Credgington, F. Hanusch, T. Bein, H. J. Snaith, and R. H. Friend, Nat. Nanotechnol. **9**, 687 (2014).
13) J. H. Noh, S. H. Im, J. H. Heo, T. N. Mandal, and S. I. Seok, Nano Lett. **13**, 1764 (2013).
14) T. Leijtens, G. E. Eperon, S. Pathak, A. Abate, M. M. Lee, and H. J. Snaith, Nat. Commun. **4**, 2885 (2013).
15) G. Niu, W. Li, F. Meng, L. Wang, H. Dong, and Y. Qiu, J. Mater. Chem. A **2**, 705 (2014).
16) R. K. Misra, S. Aharon, B. Li, D. Mogilyansky, I. Visoly-Fisher, L. Etgar, and E. A. Katz, J. Phys. Chem. Lett. **6**, 326 (2015).
17) O. A. Jaramillo-Quintero, R. S. Sanchez, M. Rincon, and I. Mora-Sero, J. Phys. Chem. Lett. **6**, 1883 (2015).
18) Y. Yamada, T. Nakamura, M. Endo, A. Wakamiya, and Y. Kanemitsu, Appl. Phys. Express **7**, 032302 (2014).
19) Y. Yamada, T. Nakamura, M. Endo, A. Wakamiya, and Y. Kanemitsu, J. Am. Chem. Soc. **136**, 11610 (2014).
20) Y. Yamada, T. Nakamura, M. Endo, A. Wakamiya, and Y. Kanemitsu, IEEE J. Photovoltaics **5**, 401 (2015).
21) Y. Yamada, T. Yamada, L. Q. Phuong, N. Maruyama, H. Nishimura, A. Wakamiya, Y. Murata, and Y. Kanemitsu, J. Am. Chem. Soc. **137**, 10456 (2015).
22) J. Even, L. Pedesseau, C. Katan, M. Kepenekian, J.-S. Lauret, D. Sapori, and E. Deleporte, J. Phys. Chem. C **119**, 10161 (2015).
23) J. A. Christians, J. S. Manser, and P. V. Kamat, J. Phys. Chem. Lett. **6**, 2086 (2015).
24) U. Rau, Phys. Rev. B **76**, 085303 (2007).
25) T. Fuyuki, H. Kondo, T. Yamazaki, Y. Takahashi, and Y. Uraoka, Appl. Phys. Lett. **86**, 262108 (2005).
26) S. Chen, L. Zhu, M. Yoshita, T. Mochizuki, C. Kim, H. Akiyama, M. Imaizumi, and Y. Kanemitsu, Sci. Rep. **5**, 7836 (2015).
27) T. Kirchartz and U. Rau, J. Appl. Phys. **102**, 104510 (2007).
28) T. Kirchartz, U. Rau, M. Kurth, J. Mattheis, and J. H. Werner, Thin Solid Films **515**, 6238 (2007).
29) A. Wakamiya, M. Endo, T. Sasamori, N. Tokitoh, Y. Ogomi, S. Hayase, and Y. Murata, Chem. Lett. **43**, 711 (2014).
30) W. H. Nguyen, C. D. Bailie, E. L. Unger, and M. D. McGehee, J. Am. Chem. Soc. **136**, 10996 (2014).
31) L. K. Ono, P. Schulz, J. J. Endres, G. O. Nikiforov, Y. Kato, A. Kahn, and Y. Qi, J. Phys. Chem. Lett. **5**, 1374 (2014).
32) N. Marinova, W. Tress, R. Humphry-Baker, M. I. Dar, V. Bojinov, S. M. Zakeeruddin, M. K. Nazeeruddin, and M. Grätzel, ACS Nano **9**, 4200 (2015).
33) H. J. Snaith, A. Abate, J. M. Ball, G. E. Eperon, T. Leijtens, N. K. Noel, S. D. Stranks, J. T.-W. Wang, K. Wojciechowski, and W. Zhang, J. Phys. Chem. Lett. **5**, 1511 (2014).
34) H. J. Snaith and M. Grätzel, Appl. Phys. Lett. **89**, 262114 (2006).
35) W. Shockley and W. T. Read, Phys. Rev. **87**, 835 (1952).
36) R. N. Hall, Phys. Rev. **87**, 387 (1952).
37) H. C. Casey and M. B. Panish, *Heterostructure Lasers* (Academic Press, New York, 1978).